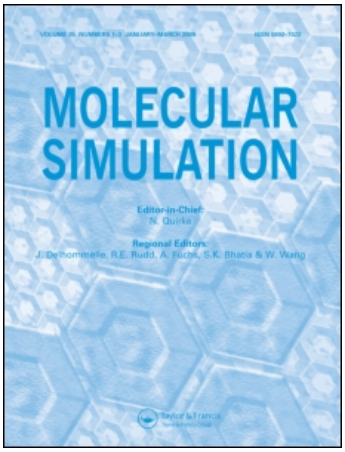

Molecular Simulation
Publication details, including instructions for authors and subscription information:
http://www.informaworld.com/smpp/title~content=t713644482

Fluctuating charge force fields: recent developments and applications from small molecules to macromolecular biological systems

Sandeep Patel[a]; Charles L. Brooks III[a]
[a] Department of Molecular Biology, TPC-6, The Scripps Research Institute, La Jolla, CA, USA

To cite this Article Patel, Sandeep and Brooks III, Charles L.(2006) 'Fluctuating charge force fields: recent developments and applications from small molecules to macromolecular biological systems', Molecular Simulation, 32: 3, 231 — 249
To link to this Article: DOI: 10.1080/08927020600726708
URL: http://dx.doi.org/10.1080/08927020600726708

Molecular Simulation, Vol. 32, Nos. 3–4, 15 March–April 2006, 231–249

Taylor & Francis
Taylor & Francis Group

Fluctuating charge force fields: recent developments and applications from small molecules to macromolecular biological systems

SANDEEP PATEL* and CHARLES L. BROOKS III

Department of Molecular Biology, TPC-6, The Scripps Research Institute, 10550 N. Torrey Pines Road, La Jolla, CA, 92037, USA

(Received January 2006; in final form March 2006)

The past decade has seen intense development of what are anticipated to be the next generation of classical force fields to be used in computational statistical mechanical approaches to studying a broad class of physical and biological systems. Among the several approaches being actively pursued currently is the fluctuating charge (or equivalently charge equilibration or electronegativity equalization) method. Within this formalism, dynamical electronic degrees of freedom are introduced and propagated in time in order to allow an electrostatic response to the local chemical environment. In this article, we present a review of our recent development and application efforts of a polarizable biomolecular force field based on the fluctuating charge formalism and founded on the CHARMM non-polarizable force field. We will discuss aspects of the parameterization, as well as recent applications to a spectrum of chemical and biological systems such as small-molecule liquid–vapor interfaces, solvated proteins/peptides, and physiological membrane systems. We will conclude with brief comments on aspects that require continued effort in terms of future development of such novel potentials.

Keywords: Polarizable force field; Biomolecules; Fluctuating charge; Charge equilibration; CHARMM

1. Introduction

There is no doubt that classical molecular simulation approaches such as Molecular Dynamics (MD), Monte Carlo (MC), and variants thereof are, today, integral components in the repertoire of tools available to computational and experimental scientists pursuing research spanning a wide range of physico–chemical systems. Within the realm of biophysics, classical statistical mechanical approaches have left a wide footprint, offering detailed, atomic-level information relevant to physiological processes otherwise unobtainable with standard experimental approaches, and thus invariably complementing the interpretation of such observations and guiding further experiment [1]. Although classical force field based methods are an invaluable tool for studying rather large biomacromolecular systems over a range of time scales, the current state-of-the-art approaches rely on empirical force fields which effectively attempt to model the subtle microscopic interactions defining the quantum mechanical energy surface. One aspect of such force fields, the electrostatic interaction, is defined by Coulomb interactions between fixed charges assigned to individual sites of the molecular construction. Due to the static nature of this representation, there is no effective mechanism for allowing an electronic response to changes in the local chemical environment. In situations involving strong anisotropy in terms of rapid variation in the chemical environment (i.e. interfacial systems, protein–solvent interface, ion conduction from bulk solution through integral membrane protein channels), one can argue that at the atomistic level, a fixed-charge representation cannot faithfully model the underlying physics. One must explicitly account for variations in electronic charge distributions (changes in classical charges as condensed representations of the molecular electronic density); as has been suggested, "…one size, in charge, does not fit all…" [2].

In response to this call, several approaches have come to fruition in the form of first-generation polarizable force fields for biological molecules (proteins, DNA/RNA, ions) [3–8]. Much as in the case of current state-of-the-art non-polarizable force fields, several options for inclusion of explicit polarizability in classical simulations have been

*Corresponding author. Tel: +1-858-784-8073. Fax: +1-858-784-8688. Email: sandeep@scripps.edu

Molecular Simulation
ISSN 0892-7022 print/ISSN 1029-0435 online © 2006 Taylor & Francis
http://www.tandf.co.uk/journals
DOI: 10.1080/08927020600726708

implemented. These include point dipole polarizable models [9], shell (Drude) models [7,10], charge equilibration models [11–13], fluctuating dipole [14], and the sum of interactions between fragments *ab initio* computed (SIBFA) [15–17], models based on molecular polarizability as introduced by Thole, and recent atomic multipole methods such as the AMOEBA [5,6] force field (implemented within the TINKER [18] modeling package). The point dipole polarizable models generally ascribe atomic polarizabilities to various sites within the molecular construct along with fixed charges, and self-consistently evaluate the induced dipole moments arising from the local electric field generated by the nearby charge density and configuration. The shell (Drude) models introduce finite-mass charged sites generally coupled to more polar nuclei via a harmonic spring with a force constant which intimately determines the local polarizability (the "atomic" polarizability in such models goes as the inverse of the force constant as one would intuitively presume); effectively, one models, locally, a system with two charges whose separation oscillates with time—a fluctuating dipole exactly. The approach, however, thus introduces extra interactions that compromise the efficiency of the algorithm. Thole-type models introduce intra- and inter-molecular dipole–dipole interactions by assigning atomic polarizabilities determined from empirical fits to experimental molecular polarizability tensors [19]. Thole introduced a damping function in order to attenuate the intra-molecular dipole–dipole interactions at short distances. The AMOEBA force field introduces permanent atomic monopole, dipole, and quadrupole moments, and explicitly treats polarization by allowing mutual induction of dipoles at prescribed sites with contributions from both permanent multipoles and induced dipoles; in this respect, an iterative approach to self-consistency is required in order to determine the instantaneous moments [5,6]. Permanent multipoles interact through a multipole interaction matrix. Atomic polarizabilities are fit to reproduce experimental molecular polarizabilities in the spirit of Thole. These values are used in conjunction with a damping scheme introduced to attenuate the intra-molecular dipole–dipole interactions in order to avoid polarization catastrophes at small separations [19,20]. Though each approach demonstrates unique advantages and shortcomings described in detail elsewhere [3,10], it currently remains to be seen if any one approach is superior to the others. In this article, we describe our efforts in developing polarizable force fields for ultimate application to force field-based molecular modeling approaches of biologically relevant systems. We will take the approach of presenting the material as a review of our recent work in this area, discussing our methodology for developing polarizable models for biomolecules as well as some recent results arising from applications to relevant biological and small-molecule systems. We aim to discuss the nature of polarizable models based on the fluctuating charge formalism in terms of bulk liquid properties, interfacial properties of small compounds, as well as novel insights arising from polarizability in the condensed phase relevant to biological systems. We will discuss systems other than water (in terms of small-molecules), thus moving away from this classic system used to study non-additive models. In Sections II and III, we describe our approach to incorporating explicit polarizability in molecular simulations of biological systems, in particular describing the protocol within the charge equilibration, or equivalently electronegativity equalization, formalism. Section IV emphasizes results from MD simulations of solvated protein/peptide systems. Section V will present work probing the bulk and interfacial properties of small-molecule alcohols, and Section VI will discuss recent work on the application of our polarizable force field to lipid and protein embedded lipid bilayer systems as a prelude to ongoing work exploring ion conduction energetics in biological ion channels. Section VII will conclude with comments on current areas requiring further work and future challenges.

2. The fluctuating charge model: electronic polarization and charge dynamics

The fluctuating charge model has been applied to various systems over the last decade [11,12,21–34]. The formalism is well documented, and the reader is directed to the relevant literature for details of the theory. Here we present an abbreviated discussion of the method and the points relevant to its parameterization and implementation within CHARMM.

The fluctuating charge method derives from the density functional theory of atoms in molecules as formulated by Yang and Parr [35]. More fundamentally, the method is founded on Sanderson's idea of electronegativity equalization [36,37]. In the density functional sense, electronegativity equalization amounts to the equalization of the chemical potential in space. In a molecule, this translates to the redistribution of charge amongst constituent atoms so as to equalize the electronegativity (electrochemical potential) at each point.

The electrostatic energy of an N-atom molecule in vacuum is:

$$E_{\text{electrostatic}} = \sum_{i=1}^{N} \chi_i^0 Q_i + \frac{1}{2} \sum_{i=1}^{N} \sum_{j=1}^{N} \eta_{ij} Q_i Q_j + \sum_{i=1}^{N} \Phi_i Q_i \tag{1}$$

The χ's are atom electronegativities (formally the Mulliken electronegativities) and are related to the chemical potential of an electron gas surrounding a nucleus by Ref. [12],

$$\mu_i = \frac{\partial E}{\partial N} = -\chi_i^0 = -e\frac{\partial E}{\partial q_i}. \tag{2}$$

The η's are the atom hardnesses. These values represent a 'resistance' to electron flow to/from an atom. The last term in equation (1) represents contributions from an external potential with ϕ being an external electrostatic potential at site *i*. We note here that in the parameterization scheme, the electronegativities and hardnesses are taken to be adjustable parameters; there is no *a priori* requirement that they equate to 'experimental' values, an approach which has been successfully demonstrated by Berne, Friesner, and co-workers in their development efforts [29].

Homogeneous hardness values are parameterized as discussed below in Section III. Heterogeneous elements are derived from the atom type values based on the combining rule [38]:

$$\eta_{ij}(R_{ij}, \eta_i, \eta_j) = \frac{\frac{1}{2}(\eta_i + \eta_j)}{\sqrt{1 + \frac{1}{4}(\eta_i + \eta_j)^2 R_{ij}^2}}, \tag{3}$$

where R_{ij} is the separation between atoms (or more generally sites) *i* and *j*, and the atomic hardness parameters are the η's. This local screened Coulomb potential has the correct limiting behavior as $1/r$ for separations greater than about 2.5 Å. This interaction is computed for 1-2, 1-3, and 1-4 sites (sites included in bonds, angles, and dihedrals). Sites separated by four or more bonds interact via a Coulomb interaction; in the case of interacting molecules, the interaction between sites on different molecules is again of the Coulomb form. We note here that an alternate model for the shielding interaction is the Coulomb overlap integral between atom-centered Slater orbitals [11,12,21]. This approximation is computationally tractable for rigid systems where the interaction matrix elements can be computed once at the start of a simulation and then used for the duration; however, for flexible systems, calculation of the overlap integral leads to non-trivial cost.

In the present case, allowing the 1–4 shielded interaction to be coupled with the functional form of the hardness (explicit dependence on nuclear coordinates) is expected to incorporate a conformational dependence of the charge distribution, a behavior that one can expect to be important in macromolecular simulations. The fluctuating charge model, in contrast to dipole polarizable models, by including explicit charge–charge interactions, incorporates higher-order multipoles which are neglected in the former case [11]. However, in certain circumstances, the symmetry of the polarizability tensor is compromised since the model is restricted to having charges at particular sites. In the case of planar molecules or molecular fragments (aromatic rings, water, etc.), out-of-plane polarization is neglected in the current implementation; however, this can be remedied by the careful addition of extra off-atom charge carrying sites (e.g. lone pairs).

Redistribution of the charge in response to changes in the local chemical environment is treated by a dynamical approach. An extended Lagrangian formalism is used to propagate the charges in time with some general charge constraint, thus strictly providing for electronegativity equalization at each dynamics step [39–42]. In the present model, molecular charge conservation is imposed; however, this can be modified to allow for charge transfer between molecular entities. In the case of proteins, or polymeric systems in general, normalization can be over physically relevant units (e.g. amino acid residues) [12].

For a system of M molecules, with N_i atoms on molecule *i*, the total energy is,

$$E(Q, r) = \sum_{i=1}^{M}\sum_{\alpha=1}^{N_i} \chi^0_{i\alpha} Q_{i\alpha} + \frac{1}{2}\sum_{i=1}^{M}\sum_{j=1}^{M}\left(\sum_{\alpha=1}^{N_i}\sum_{\beta=1}^{N_j} \eta_{i\alpha j\beta} Q_{i\alpha} Q_{j\beta} + V(r_{i\alpha j\beta})\right) \tag{4}$$

where $r_{i\alpha j\beta}$ is the distance between sites α and β on molecules *i* and *j*, respectively. The first two terms in this expression represent the electrostatic contribution, and the non-electrostatic contributions are included in the last term with $V(r_{i,j})$ including intramolecular potential terms (bond stretching, angle bending, dihedrals, etc.) and dispersion interactions of the Lennard–Jones type. The system Lagrangian with the associated constraint on total molecular charge for each molecule is then,

$$L = \sum_{i=1}^{M}\sum_{\alpha=1}^{N_i}\frac{1}{2} m_{i\alpha} r_{i\alpha} + \sum_{i=1}^{M}\sum_{\alpha=1}^{N_i}\frac{1}{2} m_{Q,i\alpha} Q_{i\alpha} - E(Q, r) - \sum_{i=1}^{M}\lambda_i \sum_{\alpha=1}^{N_i} Q_{i\alpha} \tag{5}$$

where the first two terms represent the nuclear and charge kinetic energies, the third term is the total potential energy, and the fourth term is the molecular charge neutrality constraint with λ_i the Lagrange multiplier for each molecule, *i*. The fictitious charge dynamics, analogous to the fictitious wavefunction dynamics in Car–Parrinello (CP) type methods [42,43], is determined with a fictitious charge 'mass' (adiabaticity parameter in CP dynamics). The units for this mass are (energy·time^2/charge^2). The force on a charge site then becomes the difference between the average electronegativity of the molecule and the instantaneous electronegativity at the site,

$$m_{Q,i\alpha} Q_{i\alpha} = -\frac{\sum_{\beta=1}^{N_i}(\tilde{\chi}_{i\alpha} - \tilde{\chi}_{i\beta})}{N_i}. \tag{6}$$

In terms of implementation, the charge constraint is applied by normalizing the force over the sites within a unit; that is, the instantaneous average mass-weighted force is subtracted from the instantaneous total force on each site.

3. Parameterization of the fluctuating charge model

3.1 Establishing atomic hardness and electronegativity parameters

We reiterate that the present approach to implementing the fluctuating charge model treats the electronegativities and hardnesses as empirical parameters. There is no attempt to associate the electronegativities to Pauling values (or to even relate the present parameters with each other via some electronegativity scale). One should bear in mind, also, that the lone atom electronegativities as defined in this formalism are not true isolated atom values, i.e. they are not strictly determined for single atoms in the gas phase from the atomic ionization potential and electron affinity [34].

In order to separate the fitting of the atom type electronegativities and hardnesses, the fluctuating charge model is reformulated in terms of a linear response model [22,29,44]. Equation (1) gives the electrostatic energy of a molecule in the presence of some external potential. In the absence of any perturbing external field, the last term vanishes to give

$$E^0_{\text{electrostatic}} = \sum_{i=1}^{N} \chi_i^0 Q_i^0 + \frac{1}{2} \sum_{i=1}^{N} \sum_{j=1}^{N} \eta_{ij} Q_i^0 Q_j^0 \qquad (7)$$

where the Q_i^0 are site charges in the absence of an external field.

In each case, at equilibrium, the condition that

$$\frac{\partial E_{\text{electrostatic}}}{\partial Q_i} = 0, \quad i = 1, N \qquad (8)$$

and

$$\frac{\partial E_{\text{electrostatic}}}{\partial Q_i^0} = 0, \quad i = 1, N \qquad (9)$$

must be satisfied leads to the following expressions for the cases with and without an external potential,

$$\bar{\bar{\eta}}\bar{Q} = -(\bar{\chi} + \bar{\phi}) \qquad (10a)$$

and

$$\bar{\bar{\eta}}\bar{Q}^0 = -\bar{\chi}. \qquad (10b)$$

Taking the difference of equations 10a and b yields an expression for the response of the molecular charge distribution to the external probing field

$$\bar{\bar{\eta}}\Delta\bar{Q} = -\bar{\phi} \Rightarrow \Delta\bar{Q} = -\bar{\bar{\eta}}^{-1}\bar{\phi}. \qquad (11)$$

We now have a relationship between the atomic hardness and the charge response due to the external potential. The fitting thus involves matching the charge responses computed using DFT by variation of the hardnesses.

3.2 Fitting and force field refinement

The parameterization proceeds as follows. Since we wish to maintain the CHARMM atom-typing scheme, we select a range of model compounds representing the chemical functionalities encountered in biological systems. For a given molecule, sets of 30 perturbing fields are generated. This is done by placing a dipolar probe (consisting of two oppositely charged point charges of 0.7815*e* separated by 0.5744 Å—thus reproducing the dipole moment of water) at random locations around the molecule (greater than a distance of 2.0 Å from any heavy atom of the molecule of interest) [29].

For each set of perturbations, the hardness parameters for relevant atom types are fitted to minimize the error in reproducing the charge shift upon perturbation as given by equation (11); the final hardness is calculated as the average from all sets, with the contribution from each set being weighted by the error of the fit for the set. The optimized DFT gas phase geometry is maintained for the perturbation calculations. A simple simulated annealing search in parameter space is used for the parameter optimization. No explicit constraint function for the total charge is implemented since the CHelpG-based charge differences are normalized by design. Finally, we note that there appears to be some dependence of the "convergence" of parameters on the number of perturbations (dipole probe configurations) used per set; after about 30 perturbations, values appear to converge to a narrow region of parameter space (based on test calculations for fitting to a water model).

Density functional calculations employing the B3LYP exchange-correlation functional are used to generate the electrostatic potential. The basis set, 6-31++G(2d+,p), is chosen as it was shown to be able to reproduce the gas phase dipole moment for water (1.856 D) [45]; furthermore, this level of theory is robust for reproducing gas-phase dipole moments of a variety of small molecules. This basis set adds additional diffuse polarization functions with exponents one-fourth as large as for the previous set for atoms with lone-pairs (oxygen and nitrogen) [45]. Charges for each configuration of external potential are determined by the CHelpG fit to the DFT electrostatic potential [46, 47]. Zero-field charges are determined for optimized geometries for each molecule. All DFT and electrostatic potential fitting calculations were performed using GAUSSIAN98 [48].

It should be noted that the hardness parameters are fitted in an hierarchical manner. First, the alkyl group is parameterized (methyl carbon atoms, methyl hydrogen atoms). These parameters are then carried over to the fitting of higher functional groups (alcohols, ketones, aldehydes, amides, etc.). The CHARMM22 atom typing scheme is followed without introducing any new types [49], although this constraint can be lifted for future refinement and development.

We mention here that the dipole polarizability tensor derives simply from the hardness matrix elements as

$$\bar{\bar{\alpha}} = \Delta\bar{r}\bar{\bar{\eta}}^{-1}\Delta\bar{r}^T, \qquad (12)$$

where the $\Delta\bar{r}$ are atomic coordinates relative to the center of geometry. This can be used to determine a set of hardnesses by fitting to quantum mechanically derived gas-phase or experimental (gas-phase or solution) polarizabilities. However, since the atom-centered charge representation allows for only polarization along bonds (i.e. the out of plane polarization of aromatic rings is not possible without the introduction of extra site), we opt not to include this property in the fitting scheme at this time. For a test set of 16 small molecules [4], the global average absolute error in calculated molecular polarizabilities is 8.3%, with a range falling between 1.1 and 23.5%. The predicted molecular polarizabilities for the test set are lower than the experimental isolated molecule values. Though the scaling of polarizabilities was necessary to allow for stable dynamics in the condensed phase (avoiding polarization catastrophes, for instance), the reduced polarizability in the condensed phase is physically realistic in the sense that Pauli exclusion limits the overlap of electronic orbitals (energetic penalty for electronic density overlap) in the condensed phase. This now appears to be a well-accepted empirical necessity in terms of parameterization of the current generation of polarizable force fields for condensed phase simulations [7,8,14], and represents a somewhat frustrating scenario from the perspective of the force field developer. It remains to be seen whether a direct translation of gas-phase polarization characteristics of molecules can be directly transferred to the condensed phase without the need for *ad hoc* procedures or intervention. We note that Thole-type models can afford perhaps a more direct means to couple experimental or theoretical measures of polarizability to the molecular model, as well as providing a simple means to attenuate short-range interactions in order to avoid over-polarization; however, again, these mechanisms are in essence parameterized into the model, and thus to some extent, no less *ad hoc* than the present approach. The parameterization of the atom electronegativities then proceeds by fitting to charge distributions of the optimized geometry in the gas phase (zero-field). The dipole moments are added to the objective function; this is found to be necessary to accurately reproduce the gas-phase dipole moments since they are sensitive to minor changes in the charge distribution. The electronegativities for the alkyl atom types are fitted to the ethane, propane, and butane DFT charge distributions. For the protein force field, the backbone atom electronegativities are fitted to reproduce the dipole moments and CHARMM22 charge distributions for the conformations of the blocked alanine residue, or alanine dipeptide (ALAD). Thus, the backbone carbonyl carbon, carbonyl oxygen, amide nitrogen and amide hydrogen electronegativities are determined in this way. The electronegativities for the remaining atom types are determined by fitting to gas-phase charges and dipole moments for model compounds.

3.3 Optimizing non-electrostatic parameters: non-bonded parameters

Following parameterization of the fluctuating charge model, the non-bonded contributions to the total potential are optimized in a manner which attempts to balance solute–solute and solute–solvent interactions [49]. The approach is comprised of two steps: (1) optimizing gas phase dimer geometries of model compounds (representing the range of chemical functionalities encountered in protein simulations) with water, and (2) performing condensed-phase simulations of select model compounds to monitor liquid density and enthalpy of vaporization, in the case of liquids, or crystal cell parameters and heats of sublimation in the case of crystals, as has been done by Yin and MacKerell in the development of the CHARMM force field [50] and Jorgensen and coworkers in the development of the OPLS force fields [51–53]. The first part tries to optimize the functional group–water interactions. For the present, we employ the TIP4P-FQ fluctuating point charge model [12]; this model accurately reproduces the dielectric constant of liquid water at ambient conditions and is thus satisfying to implement as a dielectric medium surrounding proteins. The second part attempts to optimize the self-interactions of the particular functional group. On the whole, one hopes to balance the solute–solute and solute–water interactions, the balance being of prime importance in maintaining the proper energetic and structural integrity of the model with respect to experimental data. Properties targeted for parameterization include the bulk liquid densities (molecular volumes) and enthalpies of vaporization, crystal cell parameters (a, b, c) and angles (α, β, γ) and heats of sublimation. For analysis, we compute vacuum versus condensed phase dipole moment distributions and structure (via radial distribution functions when experimental data is available). We emphasize that properties at one state point are targeted; thus one might argue that this effectively limits the physical range of applicability. However, most applications to proteins initially are expected to be in the vicinity of ambient conditions under which most of the liquids are studied.

The parameterization protocol is an iterative process. For a given iteration, parameters giving reasonable agreement to vacuum dimer energies and geometries are determined. Condensed phase simulations follow; the results then indicate the next direction of change for the non-bonded parameters.

The non-bonded interaction is of the Lennard–Jones type (standard in the CHARMM implementation);

$$E(R) = \sum_{ij} \mathcal{E}_{ij} \left(\frac{R_{\min,ij}^{12}}{r_{ij}^{12}} - 2\frac{R_{\min,ij}^{6}}{r_{ij}^{6}} \right) \qquad (13)$$

where the summation runs over all non-bonded atom pairs.

Bulk liquid simulations are performed on a series of liquids as listed in table 5 of Ref. [4]. Systems examined

consist of 216 molecules in a cubic periodic box simulated at constant temperature and pressure; constant temperature is maintained by a Hoover thermostat [54,55] and constant pressure via the Langevin piston method [54]. Electrostatics are treated fully via particle mesh Ewald [56,57]. We emphasize that the implementation of the FQ method as outlined here necessitates full accounting of electrostatic interactions; that is, the standard approach of electrostatic cut-offs used with fixed charge models is inappropriate. This arises from the charge normalization constraint—truncating electrostatic interactions of the sites in a defined normalization unit differently leads to incorrect forces on the charge degrees of freedom, leading to charges taking on unfeasible values. This has also been noted for dipole polarizable and earlier FQ models [58, 59]. Crystal simulations for indole and imidazole are performed using the CHARMM crystal facility with a full unit cell (four molecules in both cases) as the primary simulation unit. The crystal parameters are determined from the literature (fractional coordinates for indole [60]) and the Cambridge Structural Database for small molecules (in the case of imidazole) [61]. Charge degrees of freedom are coupled to a temperature thermostat at 1.0 K using the Nose–Hoover method [55]; the thermostat mass is 0.005 (kcal/mol/ps^2). The charges are given masses ranging between $6.9-9.0\times10^{-5}$ (kcal/mol/ps^2); this combination of thermostat and charge masses allows a stable trajectory with a 0.5 fs timestep. The timestep can be increased with a multiple-timestep algorithm as has been implemented for CPMD and classical MD [62–64]. This is ongoing in our lab at present. We note that for each system, all atoms are assigned the same charge mass, although the same atom type can be assigned a different mass among different systems. For the current work, we choose a rather small timestep to remain consistent with the selected fictitious charge masses that determine the drift from the BO surface. Currently, FQ dynamics runs require 10% more resources relative to the CHARMM22 (consistent with the original application to water by Rick *et al.* [12]) and minimizations require 3% more resources; however, due to the fact that timesteps with the FQ are limited to the regime from 0.5 to 1.0 fs versus 2.0 fs for CHARMM22, the dynamics are effectively 2–4.5 times slower. This is still competitive with point dipole models under development that report computational requirements increasing by factors up to 20 times as much as the underlying non-polarizable models [24]. As the extended Lagrangian method adopted here is analogous to the "on the fly" *ab initio* or Car–Parrinello MD methods [42], one must deal with maintaining a meta-stable state with the fictitious charge kinetic energy at a much lower temperature than the nuclear (ionic) degrees of freedom; this allows the system to remain on the Born–Oppenheimer (BO) surface where the electronic state is the equilibrium ground state for any nuclear configuration [65]. For the present implementation, strong coupling to thermostats is required to keep the charges "cold" ($\sim$1.0 K); dynamics without temperature control sees the charge kinetic energy increase to unreasonable levels quite rapidly, not unlike what is observed in CPMD for metallic systems, where the vanishing bandgap leads to little or no separation in the frequency spectra of the nuclear and electronic degrees of freedom [65,66]. Previously reported work on the application of fluctuating charge models to small molecules consistently claims weak coupling of the nuclear and electronic degrees of freedom [12,26]. This is perhaps due to the more or less rigid nature of the molecular systems with few internal degrees of freedom to which the charge degrees can couple; the present form of the shielded Coulomb interaction explicitly introduces the coupling to nuclear degrees of freedom, and the need for strict temperature control should not be surprising. The "motions" of the charge degrees of freedom can span a large range of frequencies, and overlap with the nuclear motions typically associated with classical force fields. In this sense, fluctuating charge dynamics for flexible systems requires rather strict temperature control unlike the case of rigid molecules such as water [4,67].

In the next sections, we discuss results obtained from molecular simulations using the CHARMM–FQ force field for three types of systems. The first section will deal with properties of small peptide/protein systems, the second will focus on bulk and interfacial properties of two industrially relevant fluids, and the last will discuss application of the polarizable force field to membrane systems as a stepping stone to investigating ion conduction energetics in integral membrane proteins.

4. Application to solvated peptides in polarizable solvent

4.1 Protein properties

As an initial examination of the CHARMM–FQ force field, six small peptides/proteins were selected as test systems representing realistic protein secondary structural motifs; the peptides/proteins ranged from 28–57 residues (Protein Data Bank identifications 1FSV, 1PGB, 1H8K, 1CRN, 1VII, 1ENH), thus small enough to allow extended-time MD simulations in a relatively short time to facilitate parameterization efforts [4]. In terms of protein structural stability, the CHARMM–FQ force field maintained backbone atom root mean square deviations (rmsd) from experimental structures to within 3.0 Å which is commensurate to the quality of the current fixed-charge CHARMM22 force field.

As has been observed in our, as well as others' work towards developing polarizable force fields for bulk organic liquids, one would expect to see a polarization effect in the condensed phase. To study this, we consider a simple probe of condensed-phase polarization, the average atomic charges in solution versus those of the vacuum minimized structure. Figure 1 shows plots of the vacuum versus average condensed phase partial atomic charge of backbone carbonyl oxygen, carbonyl carbon, amide

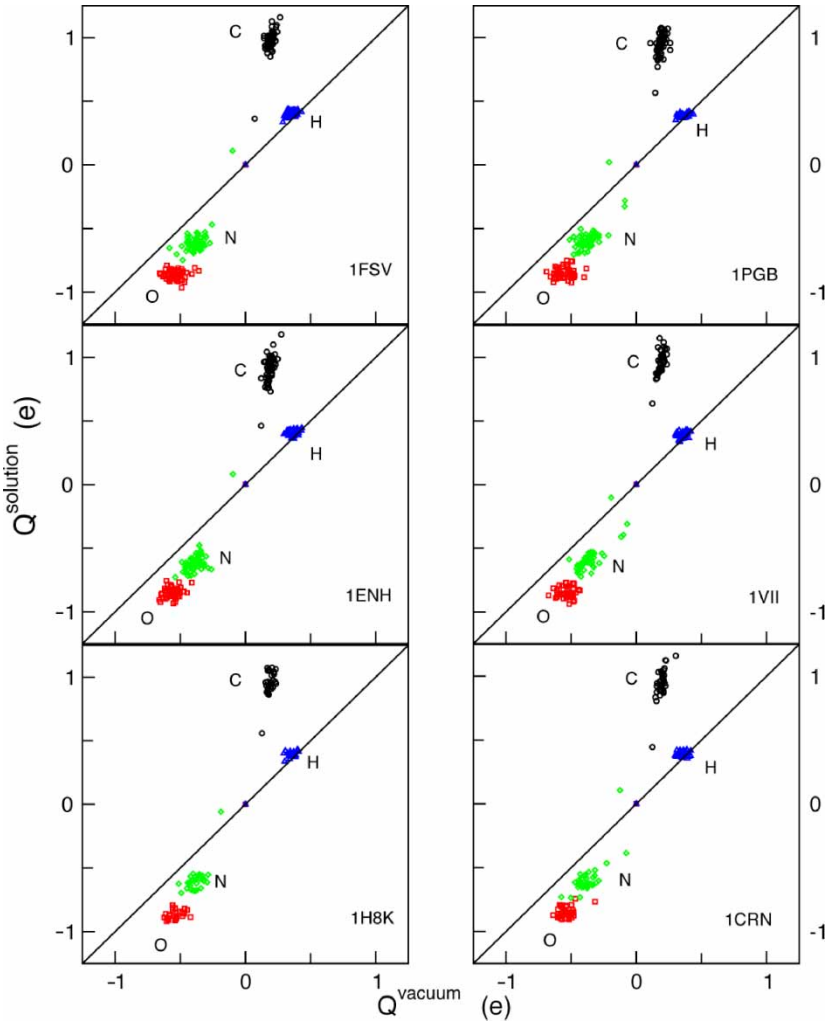

Figure 1. Comparison of condensed phase (solution) versus gas-phase charges for backbone atoms of the test proteins as named in the panels.

nitrogen, and amide hydrogen atoms for each protein. The averages are from the last 500 –700 ps of simulation, and the vacuum charges are those associated with the gas-phase minimized structure. It is clear that there is a change in condensed phase electrostatics; furthermore, it appears that more polar atoms experience a greater charge redistribution effect. We point out that, although the polar atoms as a group show a marked polarization, there is still a significant spread of the extent of polarization of individual atoms. This emphasizes the unique nature of each site, arising from the differing local chemical environments felt by each site along the protein sequence. Figure 2 shows the average charge (again from the last 500–700 ps of simulation) on backbone atoms of 1CRN (crambin) as a function of position along the chain. Clearly, an atom of a given type experiences differing environments along the backbone. The qualitative behavior seen here is in accord with the QM/MM simulation results of Liu, Yang, and coworkers [68] We note, however, that the current electrostatic model allows for more enhanced charges on atoms compared to QM/MM results; for instance, backbone oxygen atoms in the present study are in the range of −0.8 to −0.9e, while those in the QM/MM study range from −0.55 to −0.65e (and similarly for the carbon, nitrogen, and hydrogen atoms). This difference results of course from the use of different levels of theory used in the QM/MM procedure and our protocol to fit the electrostatic model parameters; in essence, the charge basis is different and in part leads to the variance in charges. Interestingly, the fluctuations in atom charges based on the FQ force field (on the order of 0.01– 0.05 e) are commensurate to those observed with the QM/MM treatment. This suggests that the hardnesses, which in one sense represent a harmonic restraint on charges (a quadratic energy penalty for drift away from the electronegativity equalizing distribution), allow a more or less valid fluctuation of charges. It is important to note that while it is true that at equilibrium the charges at individual sites fluctuate around an average value, thus making an argument for treating the electrostatics at a given site with an average fixed charge, the power of non-additive force fields is to allow for rather drastic changes in environment such as from an unfolded to folded state or between the interior and exterior of a large protein. Finally, apart from a sequence dependence on charge, there does not appear to be any discernible trend; for instance, one might expect

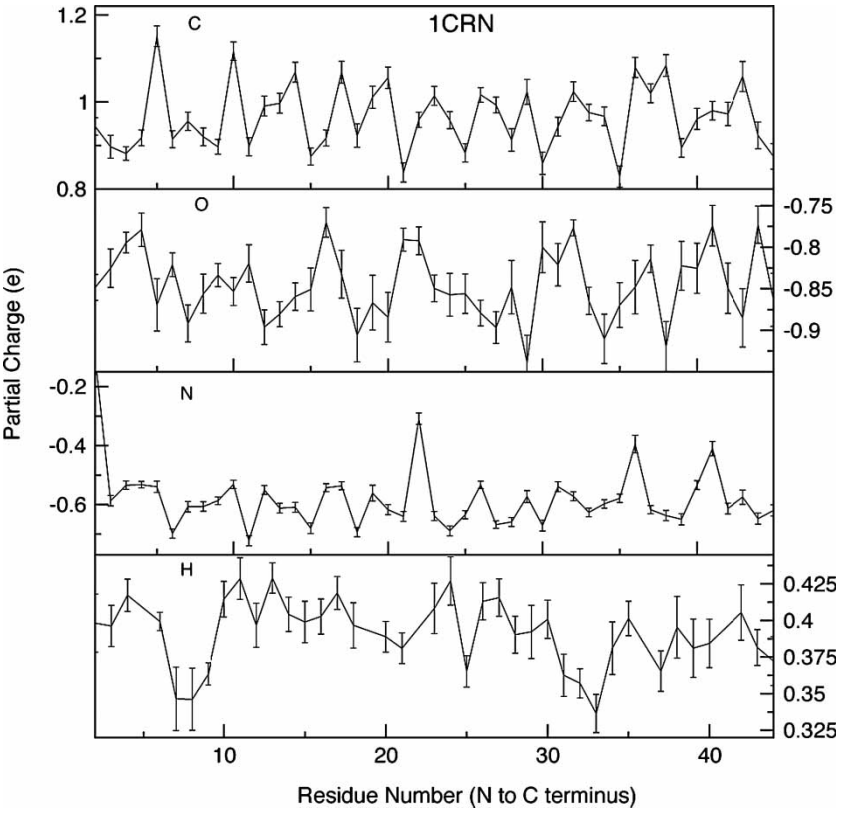

Figure 2. Dependence of average partial charge on the backbone atoms of crambin (PDB:1CRN).

differences between sites in different secondary structural elements, or perhaps between buried and exposed residues. The lack of such behavior may be simply due to the relatively small protein sizes tested, where essentially the entire protein/peptide is "exposed" to solvent.

4.2 Water properties: dipole moment distributions

It is well documented in the literature that water near interfaces (i.e. vicinal water) exhibits unique properties relative to the bulk. In the present simulations, one can consider the nature of water molecules in the vicinity of the solvated peptide. Specifically, we ask about the distributions of water molecular dipole moments as one moves away from specific sites along the protein backbone. For the present analysis, we investigate the distributions as a function from backbone carbonyl oxygen and amide hydrogen atoms, as these sites are usually involved in strong hydrogen-bonding interactions with solvent. In our previous work, as well as results reported by Rick *et al.* on amide solvation, water molecules within the first solvation shell exhibit a shift towards higher dipole moments by about 0.1– 0.2 Debye. For the present analysis, water molecular dipole moment distributions are computed in shells, around the backbone carbonyl oxygen, from (1) 1.5 to 3.0 Å, (2) 10.0 to 12.0 Å, and (3) 16.0 to 17.0 Å (essentially bulk). Figure 3 shows the distributions for each protein. The distributions for all proteins look remarkably similar, and this is not too surprising since these are averaged over all carbonyl oxygen atoms that, in terms of electrostatics (charges), are for the most part equivalent. There is a systematic polarization of water molecules within the first two solvation shells (1.5–3.5 Å), up to on the order of 0.2–0.3 Debye; with concurrent polarization of the backbone oxygen atoms. This is consistent with the shift observed for TIP4P-FQ water molecules in the first solvation shell around N-methylacetamide as reported in earlier work [4,11]. One obtains the bulk-like distribution moving outward towards the bulk. It is interesting to note that there appears to be intermediate shells of water displaying distributions in between those of the bulk and first-shell, implying a gradual shift in dielectric environment (high dielectric to low dielectric) moving away from the protein-solvent interface. Although this appears to be a quite subtle behavior, it is counter to most current implementations of implicit solvation models for proteins that invariably invoke sharp dielectric boundaries. The sharp peaks at roughly 2.87 Debye result from water molecules within the first solvation shell that are directly hydrogen bonded to the carbonyl oxygen atoms; more specifically, this is a subset of molecules with carbonyl oxygen to water hydrogen distances from 1.7 to 1.8 Å. Furthermore, this strong association with solvent occurs predominantly between carbonyl oxygen atoms associated with residues not involved in protein-protein contacts stabilizing helical and sheet structures. Finally, there is a contribution from water molecules donating to two

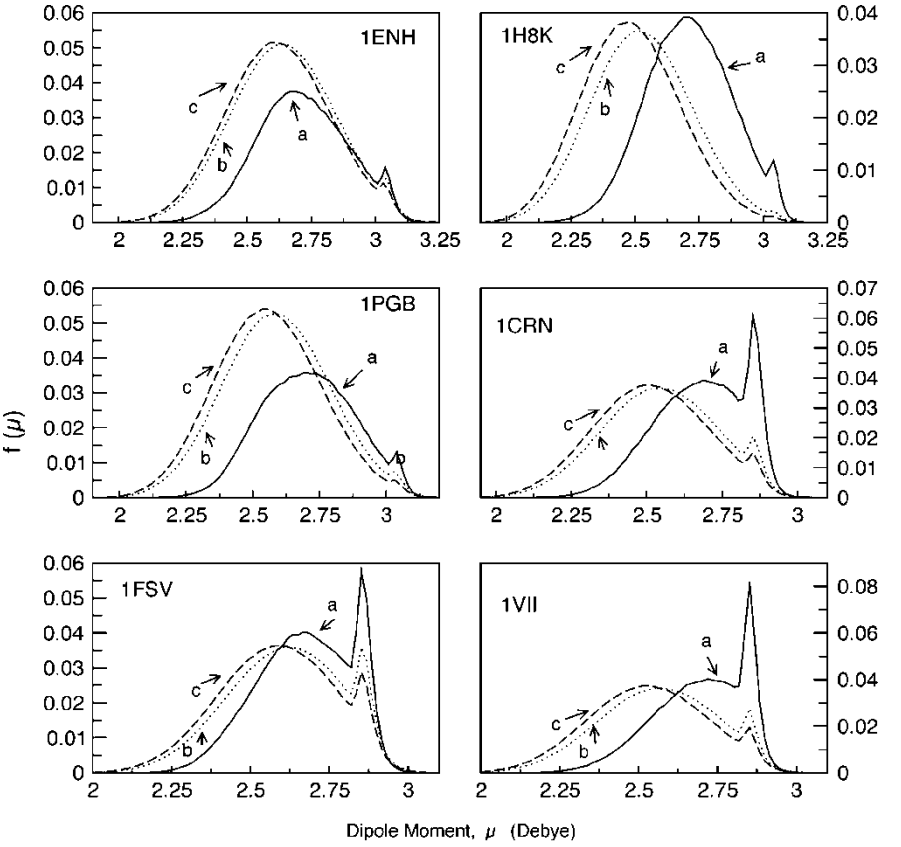

Figure 3. Distributions of water molecular dipole moments for water molecules coordinating with the backbone carbonyl oxygen atoms. Curves labeled "a" are for water molecules within 3.0 Å of oxygen atoms. Curves labeled "b" represent water molecules 10–12 Å away from oxygen atoms, and curves labeled "c" represent water molecules in the bulk.

hydrogen bonds, a scenario one would expect to give rise to strong polarization.

5. Probing bulk and liqud–vapor interfacial properties of alcohols

Alcohols such as methanol and ethanol play a significant role as industrial solvents for myriad chemical processing applications; moreover, their properties over a wide range of thermodynamic states are exploited in applications such as catalyst-free conversion of rapeseed oil (and other fatty acids) to biodiesel fuel in supercritical methanol [69], efficient separation technologies such as supercritical fluid chromatography, and recycling of polymers such as polysiloxane and polyethyleneteraphthalate (PET) under supercritical methanol conditions [70]. Liquid methanol is fundamentally interesting from a chemical physics perspective as it is an analogue to water, with a methyl group replacing one hydrogen atom, a minor substitution allowing for rather significant differences between the two hydrogen-bonding liquids. For instance, in the bulk, methanol coordinates as clusters of chains or small rings as opposed to the well-known tetrahedral structure of bulk water. An early theoretical study of the free surface of methanol described methanol as the simplest surfactant model due to the juxtaposition of the hydrogen-bonding hydroxyl and aliphatic methyl groups [71]. This feature of the molecule leads to a rich liquid–vapor interfacial structure with the aliphatic tails projecting towards the vapor phase [72,73].

Along with its widespread use in the chemical processing industry, ethanol is also interesting from a chemical physics perspective. Due to its strongly associating nature (hydrogen bonding propensity), ethanol shows a unique structure in the liquid; unlike the tetrahedral structure of water, though, this structure has recently been suggested to consist predominantly of winding chains much like in methanol [74]. In light of these results, there is current supposition of a transition from a chain-like bulk phase structure to one dominated by small clusters as recently determined for methanol in the supercritical regime [75]. Furthermore, the close juxtaposition of hydrophilic and hydrophobic moieties leads to anomalous behavior upon mixing of simple alcohols and water; recent experimental [76] and theoretical/simulation [77] studies have directed attention to the solvation structure around the aliphatic and hydroxyl groups of ethanol in order to account for the anomalous mixing properties of the two fluids. Recently, non-linear optical methods such as vibrational sum frequency generation (VFSG) and second harmonic generation (SHG) have uncovered the preferential orientation of ethanol at the pure liquid–vapor interface.

Table 1. Comparison of selected bulk liquid properties for methanol and ethanol computed using several available potential functions.

Liquid properties	FQ-methanol	CHARMM (additive)	OPLS[†]	AMBER[‡]	PIPF[¶]	Dang *et al.*[§]	Experiment
				Methanol			
ρ (g/cm^3)	0.809±0.002	0.762	0.759±0.003	0.81	0.747±0.005	0.797±0.01	0.787[‖]
$\Delta H_{vap.}$ (kcal/mol)	8.90±0.02	9.13	9.05	8.5	9.0±0.02	9.10±0.2	8.94[‖]
D_{self} (cm^2/s)	2.39±0.073	2.0	–	2.65	–	2.38±0.1	2.42[#]
γ (dyne/cm)	19.66±1.03	22.3	–	–	–	25±2	22.6[††]
μ_{liquid} (Debye)	2.42±0.014	2.37	–	–	2.42	2.81±0.05	2.87[‡‡]
				Ethanol			
	FQ-ethanol	CHARMM (additive)	OPLS	PIPF[C]	Experiment		
ρ (g/cm^3)	0.787±0.001	0.791±0.001	0.748±0.003[A]	0.759±0.002	0.785[E]		
$\Delta H_{vap.}$ (kcal/mol)	10.24±0.18	10.30±0.1	9.99±0.02[A]	10.08±0.01	10.11[E]		
D_{self} (10^5cm^2/s)	0.96±0.03	0.95±0.09	1.56[B]	1.09	1.0[F]		
γ (dyne/cm)	22.74±0.64	23.701±0.47	19±1.0[C]	–	22.8[G]		
μ_{vacuum} (Debye)	1.63	2.36	2.2[A]	1.87	1.69[H]		
μ_{liquid} (Debye)	2.207±0.001	2.36	2.2[A]	2.44	3.04[D]		
ε (dielectric permittivity)	20.64±0.28	17.1±0.6	16.1[A]	23.9	24.3[I]		

[†]Reference [106].
[‡]Reference [107].
[¶]Reference [9].
[§]Reference [108].
[‖]References [109]
[#]Reference [110]
[††]References [111]
[‡‡][H]Reference [112].

In terms of bulk properties, the fluctuating charge models for these two alcohols accurately reproduce a range of properties of the condensed phase as shown in table 1; also shown are predictions from earlier polarizable and non-polarizable force fields. An interesting behavior of the polarizable models is the condensed phase induced dipole moment as demonstrated by the distribution of molecular dipole moments shown in figure 4. This enhancement is unique to force fields capable of allowing polarization in some fashion, whether it is a full quantum mechanical treatment as in the case of *ab initio* MD (Car–Parinello dynamics). Upon close inspection, the data for methanol show a bimodal distribution of moments similar to that observed in a recent study of pressure effects on the hydrogen-bonding structure of liquid methanol using a dipole polarizable methanol force field [78]. The shoulder at smaller values of the dipole moment arises from contributions from methanol molecules not involved in hydrogen-bonding interactions. This is a rather subtle effect that the polarizable models capture, and it is rather encouraging that this is a property seemingly universal to diverse approaches (charge equilibration, point dipole polarizability) to electronic polarizability in classical molecular simulations.

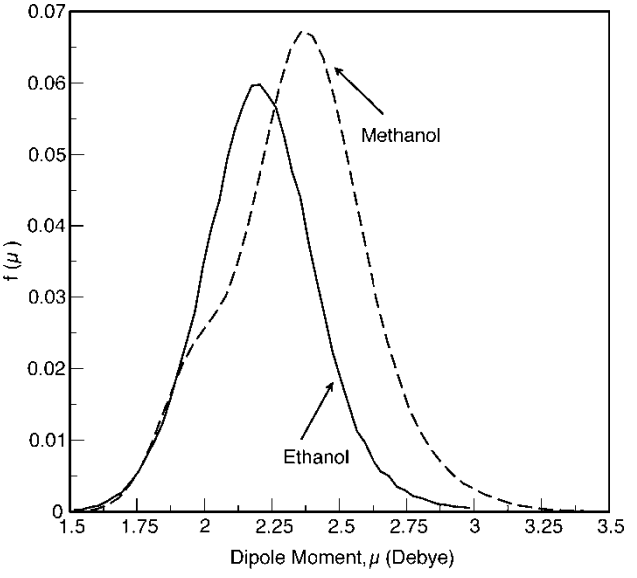

Figure 4. Distributions of molecular dipole moments for ethanol and methanol in the bulk liquid.

In terms of interfacial properties, the polarizable models are generally in good agreement with experimental surface tension values; furthermore, the models capture the interfacial orientational structure as observed via VSFG and SHG spectroscopies. These results are also consistent with the results of earlier potentials for alcohols [13]. Where the polarizable model departs from the fixed charge models is in the ability to model the monotonic decrease of the average molecular dipole moment from the condensed phase value to the gas-phase value as shown in figure 5. A further difference with respect to fixed charge force fields is seen when considering the dipole potential through the liquid–vapor interface. Figure 6 shows the

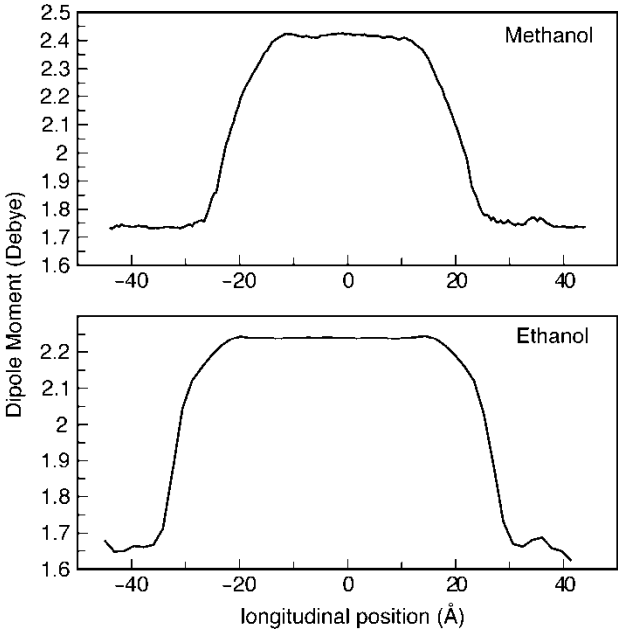

Figure 5. Profiles of the average molecular dipole moment of methanol and ethanol molecules. The central region represents bulk liquid, with the regions at either extreme depicting the coexisting vapor phase.

profiles for methanol and ethanol, as well as that through the interface computed using the CHARMM22 nonpolarizable force field.

A final consideration with respect to the small-molecule systems is the prediction of the vapor–liquid equilibrium curve and subsequent prediction of the critical properties (temperature, density). From vapor–liquid equilibrium coexistence densities (figure 7) computed using canonical MD simulations coupled to renormalization group theory,

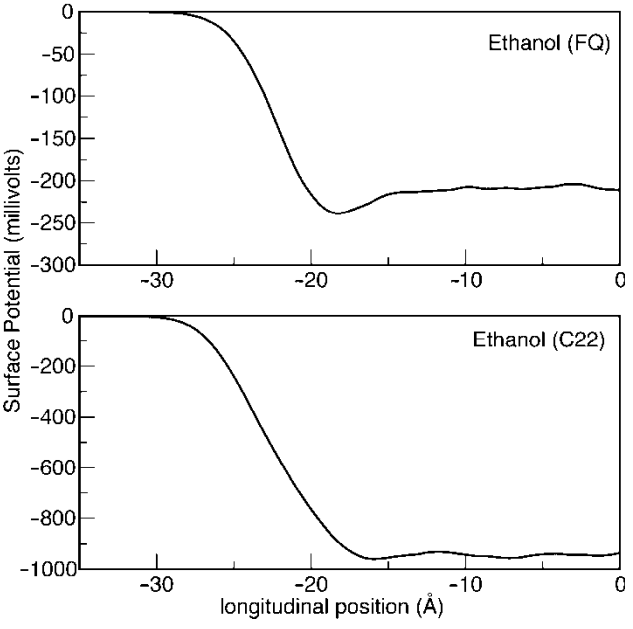

Figure 6. Dipole surface potential for ethanol. Results shown for the polarizable (FQ) model (top panel) and the non-polarizable CHARMM param22 model (bottom panel).

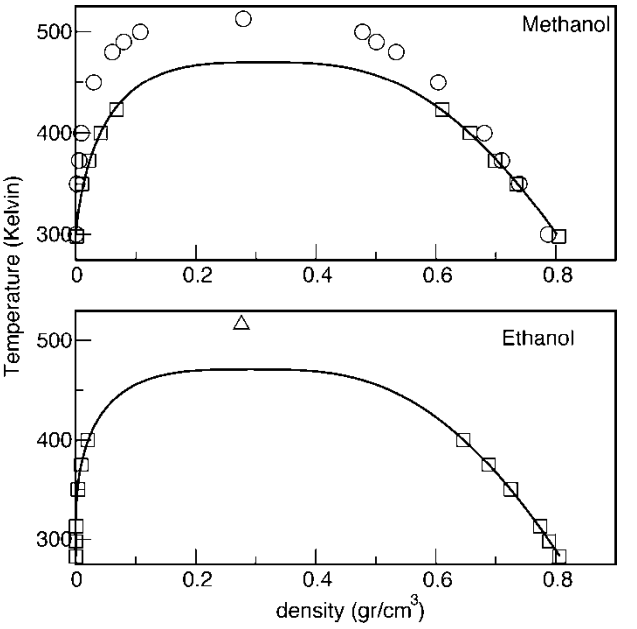

Figure 7. Temperature–density vapor–liquid coexistence curves for methanol and ethanol. The top panel shows data for methanol, with the circles representing experimental data, the squares the simulation data, and the solid line a fit to the simulation data. The bottom panel shows the simulation data for ethanol (squares), a solid line representing a fit to the simulation data, and a diamond representing the experimental critical point.

the critical density and temperatures can be estimated. For the FQ models developed in our laboratory, the critical temperatures for methanol and ethanol are 470.1 and 470.84 K, respectively. The experimental values are 512.65 and 516.25 K, respectively. The non-polarizable CHARMM22 force field predicts 476.4 and 486.11 K for methanol and ethanol, respectively. For the critical densities, the polarizable model predicts values of 0.312 and 0.291 g/cm^3 for methanol and ethanol, respectively. The experimental values are 0.279 and 0.276 g/cm^3, respectively, and the CHARMM22 force field predicts 0.273 and 0.284 g/cm^3. In general, the polarizable and non-polarizable models are equivalent in terms of the current vapor–liquid equilibrium predictions. It is, however, important to keep in mind several key points. It is our belief that the comparison of classically polarizable force fields that must incorporate lower polarizabilities for the low-density phases generally in equilibrium with the condensed-phases is not truly valid. It is accepted from a theoretical perspective that the polarizability of a molecule in the vacuum (isolated molecule) is higher than in the condensed phase [79,80]. Thus, polarizable models using a single description of molecular polarizability for both phases should not be expected to perform well in terms of reproducing all condensed phase and gas-phase properties simultaneously with vapor–liquid equilibrium. The attractive electrostatic contribution arising from polarization of the low-density phase falls off too quickly for polarizable models as the critical point is approached. It still remains to be seen whether some explicit accounting for this effect (which in

all respects is truly physical) will result in more quantitative vapor–liquid equilibrium behavior for polarizable models. There are quite successful classical polarizable force fields currently described in the literature [25,81]. These force fields are in general based on polarizabilities lower than the gas-phase value; these models are then parameterized with the entire vapor–liquid coexistence curve as a fitting objective. Furthermore, accuracy in the vapor–liquid equilibrium prediction comes with a price in terms of other properties related to the condensed phase (i.e. liquid microstructure in the case of water is misrepresented in the POL-1 and POL-2 models of Chen *et al.* [25]). There is ongoing work in our laboratory exploring the consequences of models using environment (or phase-dependent) polarizabilities for phase-equilibrium calculations.

6. Towards modeling of membrane ion channel systems: MD simulations of DMPC-water bilayer and DMPC-water-gramicidin A systems

With the increase in computational resources and advances in theory, there has been an accelerated drive towards more quantitative descriptions of biophysical systems, and in particular, ion channel systems [82–87]. At the very least, the nature of the fundamental physics governing macroscopically observable processes is sought to more quantitative degrees. Recent studies of cation translocation energetics through the Gramicidin A (gA) [40,88–90] ion channel (an anti-bacterial peptide) suggest that modern non-polarizable force fields are inadequate for quantitatively reproducing the free energy surface underlying the conduction process; the specific culprit is invariably the lack of explicit polarizability in standard state-of-the-art force fields. The polarization of local coordinating backbone dipoles as well as of channel water molecules is conjectured to play a significant role in facilitating the conduction [91]. It thus appears that narrow, highly selective ion channels such as gA are rigorous testing grounds for next-generation force fields. To approach the problem of investigating ion conduction energetics in gA, work in our laboratory has begun to explore the applicability of polarizable force fields to hydrated membrane and hydrated integral protein systems. As mentioned in the previous sections, our laboratory has developed a first-generation protein force field coupled to a polarizable water force field developed independently. As work continues on developing polarizable models for phospholipids, we have begun to explore application of the current polarizable water and protein force fields to mixed systems consisting of polarizable protein and solvent, and non-polarizable phospholipids. In the next sections, we discuss results pertaining to the applicability and unique properties of these systems arising from the introduction of protein and solvent polarizability.

6.1 DMPC bilayer in TIP4P-FQ solvent

Together with the ongoing work toward developing a fully polarizable atomistic phospholipids force field, parallel studies have been performed probing the validity of implementing mixed polarizable and non-polarizable (FQ/MM) potentials. In this case, the membrane is the only component treated with a fixed-charge force field; solvent (taken to be the TIP4P-FQ model of Rick *et al.* [12].) and protein (taken to be the CHARMM–FQ force field, Patel *et al.* [4]) are treated as explicitly polarizable.

Prior to undertaking calculations on the full membrane/protein system, initial calculations of the DMPC (dimyristoyl phospatidylcholine) bilayer solvated with explicit polarizable water were performed. For the simulations, a bilayer geometry of 96 DMPC molecules was solvated with the TIP4P-FQ water as solvent; the initial geometry was generated from a snapshot of an equilibrated trajectory using the non-polarizable force field with TIP3P water as solvent. The membrane was fully based on the standard CHARMM param27 force field parameter set [92]. Slight modifications to the existing CHARMM [93] program were necessary to allow a consistent application of the FQ approach to mixed systems. Simulations for this test case were run in the canonical ensemble. In what follows, we discuss some properties and comment on the validity of the mixed "FQ/MM" approach in analogy to QM/MM approaches where the QM region rigorously allows for charge response (polarization) to the local environment as does the classically polarizable model.

Figure 8 shows density profiles of various components of the membrane–solvent system; the profiles display the typical distributions of the various membrane components on moving from the membrane interior to bulk. Interestingly, the width of the interface is greater than that obtained using a fixed-charge force field. Also, there is a non-trivial penetration of water molecules into the membrane interior, as is also observed with non-polarizable models in terms of the formation of transient water wires through the channel [94]. Further considering the solvent, figure 9 shows a profile of the molecular dipole moment of water going from the bilayer interior to the bulk. As one would expect, the water model captures the effect of local environment as demonstrated by the monotonic increase of the average molecular dipole moment from a near-vacuum value of about 1.9 Debye, to the average bulk value of 2.5–2.6 Debye. The value of the dipole moment in the bilayer interior approaches the gas-phase value as the effective dielectric of the membrane is underestimated by non-polarizable force fields. Interestingly, novel polarizable force fields for this class of molecules are now encouragingly demonstrating the ability to quantitatively capture the dielectric response of these systems [95,96].

Considering the properties of the membrane, we focus specifically on deuterium order parameters (and specifically the variation of this parameter with position along

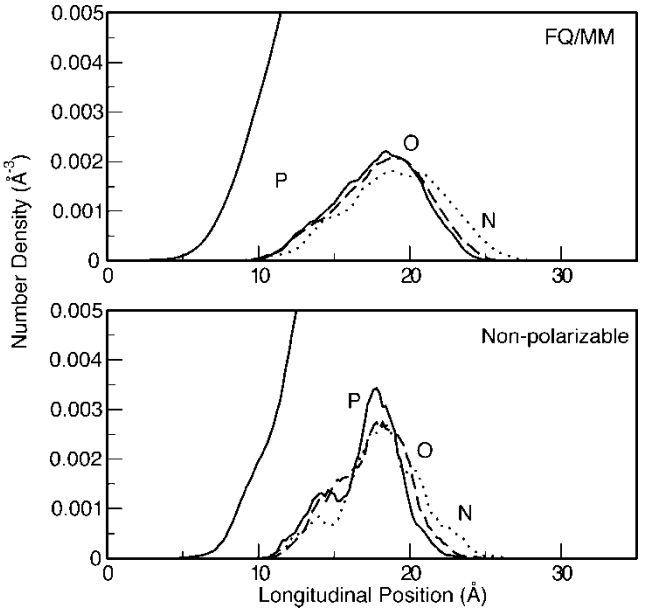

Figure 8. Number density profiles for the water, phosphorous, oxygen, and nitrogen atoms of the phospholipids headgroup moieties. The top panel shows data from MD simulations using the mixed FQ/MM formalism, while the lower panel shows results from simulations using the additive CHARMM27 force field.

the lipid backbone), which can be compared to experimental data and are often taken as a strong benchmark for force fields for membrane lipids. Figure 10 shows the Sn-2 and Sn-1 chain order parameter profiles along the lipid chain. It is evident that the standard force field is not perturbed by the presence of the polarizable solvent; the profiles are also in accord with experimental measurements [97].

6.2 DMPC—TIP4PFQ—gramicidin A

We next consider simulations of gA in a DMPC bilayer solvated by polarizable TIP4P-FQ water. This work will allow further testing of the polarizable protein model as well as give some insight into novel, albeit subtle, properties of the system observable only with polarizable force fields. The system consists of the gA dimer embedded in a bilayer comprised of 20 DMPC molecules, the whole construct then solvated by TIP4P-FQ water. Periodic boundary conditions with a hexagonal geometry are applied; the hexagonal geometry is chosen for purposes of computational expediency (the simulations reported below employ a time step of 0.5 fs). The channel simulations are carried out in the NPT ensemble; simulations using the mixed force field span 5 ns, while the non-polarizable force field runs represent 1 ns and are shown for reference.

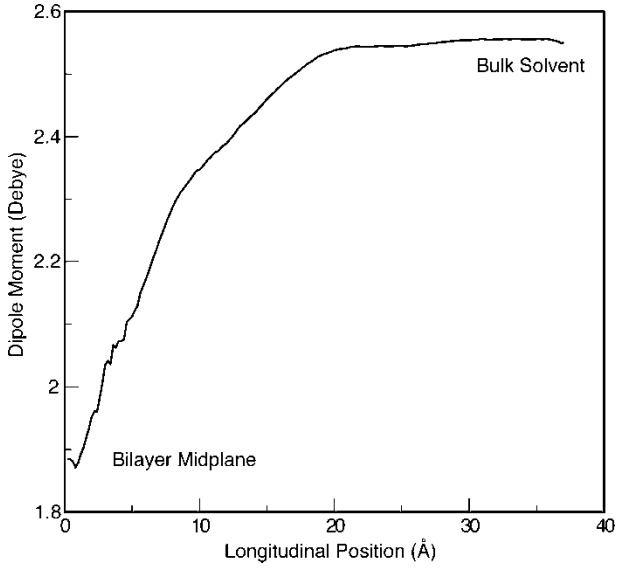

Figure 9. Profile of the average molecule dipole moment of water from the bilayer midplane to the bulk solution.

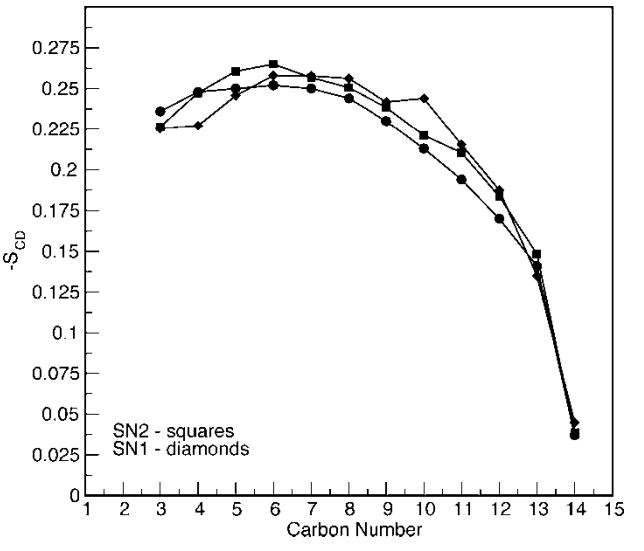

Figure 10. Profiles of the deuterium order parameter for the SN-1 and SN-2 chains of DMPC from MD simulations using the mixed FQ/MM force field. Experimental data are shown with circles.

A primary concern, as with simulations of solvated proteins at ambient conditions, is stability of protein structure over long time scales relative to crystallographic structure. Figure 11 shows the backbone rmsd profile for both dimers of the gA system (relative to the X-ray structure of Townsley *et al*. [88]). It is evident that the structure is maintained over the 5 ns run; the fluctuations in rmsd are equivalent to those allowed by the standard CHARMM force field. Taking the surface area of the gA to be the canonical value of 250 $\AA^2$ [98], the area per headgroup for the DMPC model is determined to be 57.2 $\AA^2$, in sufficient agreement with experimental data of 59.6 $\AA^2$ [82] figure 12.

Figure 13 shows density profiles for the components of the membrane and water. It is worthy to note that the water density profile within the channel suggests a slower dynamics of channel water molecules, predominantly due to the enhanced interaction arising from mutual polarization of the protein backbone and water dipoles as will be discussed below. Figure 12 shows the deuterium order parameter profiles for the Sn-2 chain which are again in agreement with experiment; the FQ/MM simulation results are in excellent agreement with experimental results on a 15:1 DMPC:gA system [98]. There is enhanced order imposed by the presence of the protein, particularly near the headgroup regions.

As suggested above, the polarizable force field should allow for polarization effects explicitly, and at this point, we consider the differing water electrostatic properties in the various local environments of the system. Figure 14 shows distributions of the molecular dipole moment in the bulk and channel interior, which show a marked difference. The bulk water molecules display a broad distribution of dipole moments, whereas the channel waters reflect a more homogeneous environment in the channel interior; moreover, there is a shift in the distribution to a slightly higher value of the dipole moment. This is consistent with the observations for TIP4P-FQ water molecules vicinal to amides in solution. This behavior is also consistent with the interaction of the enhanced water dipole moment with the larger backbone

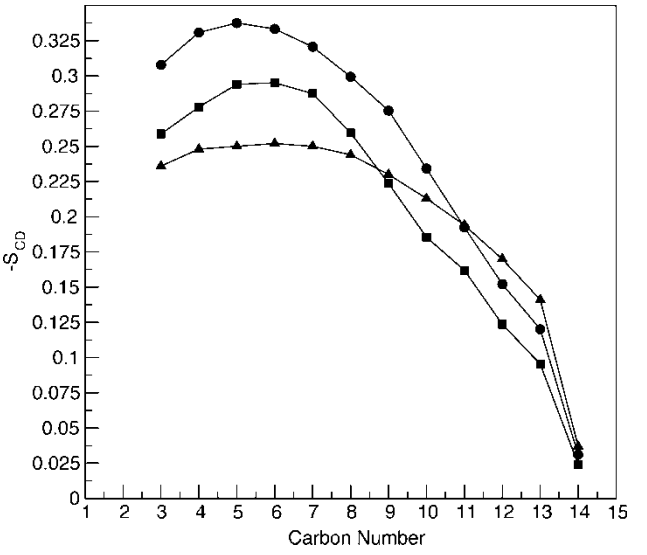

Figure 12. SN-2 chain deuterium order parameters. The curve with triangles is the experimental data for the pure DMPC bilayer. The curve with square symbols represents results from MD simulations using the mixed FQ/MM force field (polarizable gA and water with non-polarizable lipid). The curve with circles represents results of a simulation using the fully non-polarizable CHARMM27 force field.

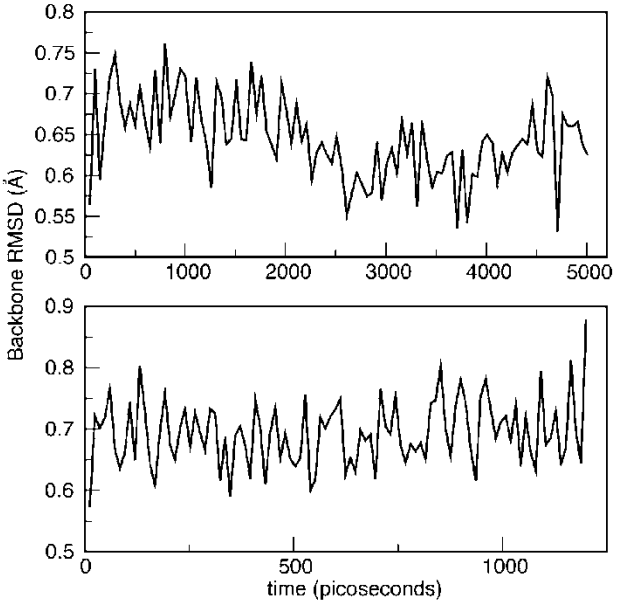

Figure 11. Backbone root mean square deviations (rmsd) versus time for gramicidin A (gA). The top panel shows results using the mixed FQ/MM force field. The bottom panel is from a simulation using the non-polarizable CHARMM27 force field.

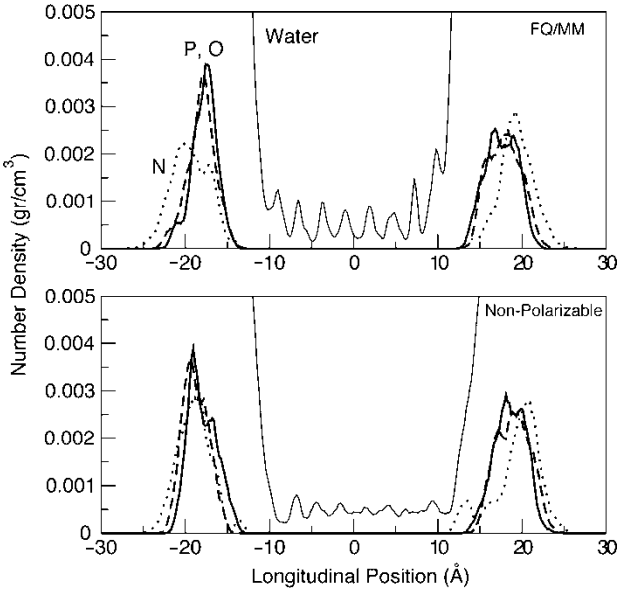

Figure 13. Number density profiles for water, nitrogen, phosphate, and oxygen atoms for the FQ/MM and non-polarizable force field simulations of gA in hydrated DMPC.

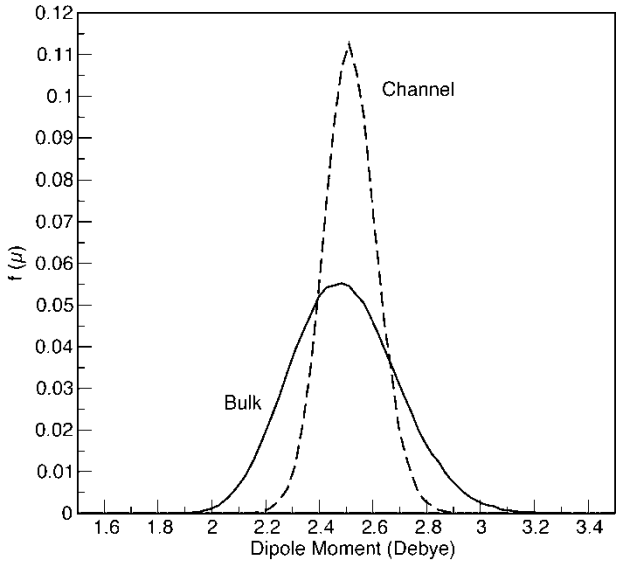

Figure 14. Distributions of water molecular dipole moments in channel interior and bulk solution.

carbonyl dipole moment, and in this sense reflects the ability of the explicit polarization incorporated in the force field to account for the local chemical environment, mutually for both the water and peptide moieties.

Finally, we consider the electrostatic properties of gA by considering backbone carbonyl dipoles. Figure 15 shows the carbonyl backbone dipole moment as a function of residue going from the center of the dimer out to the bulk solvent. The inner region of the channel shows a fairly uniform dipole moment, but the major difference arises with respect to outer residues having the opportunity to participate in multiple interactions with solvent. The polarizable force field captures the subtle difference (in electrostatics) of carbonyls polarized by varying degrees of coordination with water molecules. In terms of the conduction process for cations through the channel, this behavior suggests that polarizability of these relevant moieties should provide a means to attenuate internal barriers to a cation translocating through the channel. The response of the backbone carbonyl dipoles coupled to that of the ion-coordinating channel water molecules will certainly bear on the energetics of cation transport through the channel.

7. Conclusions and future directions

In this article, we have discussed our recent progress in the area of development and application of polarizable force fields for biological molecules. In particular, we have addressed our parameterization strategy, as well as the application of our fluctuating charge force fields to study systems ranging from simple, industrially relevant fluids (methanol, ethanol) to large macromolecular assemblies such as lipid bilayers and integral membrane proteins. For the most part, this early work has been in the spirit of proof of concept and has laid the foundation for exploring more complex systems. The addition of a further level of physics has allowed for a novel set of physical behavior described using classical simulations. In the case of small molecules, allowing a simple representation of polarizability allows for a strong condensed phase effect in terms of enhanced molecule dipole moments which self-consistently shift to higher values relative to the isolated-molecule case simply with the use of a single parameterization, a physical behavior not described using fixed-charge force fields. This is explicit in the case of interfacial systems, such as pure liquid–vapor interfaces, where our work on small-molecule alcohols has shown the monotonic decrease of molecular dipole moments from the

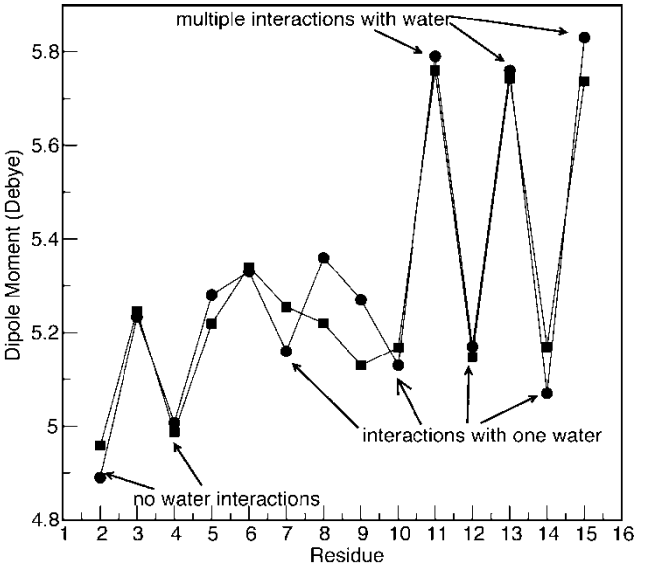

Figure 15. Variation of backbone carbonyl dipole moments along the gA dimer. The profile is shown from the center of the channel towards the bulk solution on the right. The two curves represent the two dimers.

condensed phase value to the vapor phase value. Application of the first-generation force field to protein/peptide systems allows for the polarization of protein, as evidenced by the enhanced condensed-phase charges relative to vacuum; furthermore, for a given protein/peptide, there is a sequence-dependence of the partial atomic charge as one would expect, and is observed in low-level quantum mechanical tight binding simulations of small proteins such as crambin [68] and QM/MM calculations probing the folding pathway of betanova [99] and cold shock protein A (cspA) [100]. This may be a subtle matter for gross properties, but the ability to capture charge redistribution in response to differing chemical environments, such as is the case along the protein backbone, should be important in understanding enzyme catalytic properties or chemical reactivity and/or specificity. Furthermore, the protein–solvent interface displays unique properties in terms of the enhanced electrostatics of water molecules vicinal to the protein, in keeping with earlier studies of solvent dipole moment enhancement in the vicinity of polar solutes such as N-methylacetamide in water [11]. Finally, we have presented results of MD simulations of hydrated pure lipid bilayers as well as of the bacterial ion channel Gramicidin A (gA) embedded in DMPC lipid bilayers; this work lays the foundation for pursuing investigations of the ion conduction energetics in the gA channel where it has been conjectured that polarizability will lead to more quantitative connections to experimental observables. We have demonstrated the application of a mixed fluctuating charge—fixed charge model (FQ/MM) for modeling of pure and protein-embedded lipid bilayer systems; our models involve polarizable models of solvent and protein in conjunction with fixed-charge lipid models. These simulations are the first to use classical polarizable protein force fields for probing biologically relevant systems.

The field of polarizable force field development is now witnessing rapid growth as several groups are pursuing fully self-consistent models for biomacromolecules [3,4,6,7,24,101,102]; in fact, each of the major players has a first-generation force field available for small molecules as well as, in limited cases, proteins, DNA/RNA, and cationic and anionic species. It has been suggested recently that, "…there will be continued development and increased use of polarizable force fields" [103]; furthermore, "…there will be reduced effort devoted to development of nonpolarizable force fields" [103]. Although the latter statement may prove controversial within the current modeling community, it is certain that in the next phase of the history of polarizable models, we believe that detailed characterization of polarizable force fields will be necessary in order to determine the strengths and weaknesses of each of the diverse approaches to polarization now in place. Characterization of these models will require determination of solvation free energetics for a wide array of compounds (representative of the chemical environments in biological systems). This is much in the spirit of recent calculations of free energies of amino acid analogs [103,104] that have set the target for the accuracy to reproduce or better.

In terms of practical applicability, one of the major issues will be to increase the efficiency of polarizable force fields to be competitive with current state-of-the-art fixed charge force fields. In the case of the fluctuating charge models, the bottlenecks arise due to the smaller timesteps required in order to propagate the significantly lighter charge degrees of freedom in order to remain on the Born–Oppenheimer surface during dynamics within the extended Lagrangian formulation. An approach that may prove fruitful is the propagation of charge normal modes separately from the explicit nuclear degrees of freedom [67]. Although this approach may not be feasible for flexible systems where the normal modes can change with conformation, or may require more complex strategies for dynamics, it may be of use via mixed propagation of systems composed of rigid and flexible components (flexible protein with rigid water model, for instance) [67]; this type of approach would certainly offer more efficiency for fully solvated systems for which the time devoted to dynamics of the explicit solvent represents a majority of the computational load.

Furthermore, for the fluctuating charge models, due to the requirement for a full accounting of the long-ranged electrostatic interactions via some variant of an Ewald summation, multiple time-step methods incorporating correct decompositions of the dynamical propagator will be required. Recent work suggests that separating the short-range contributions arising from the reciprocal space sums in Ewald based methods which is the correct decomposition of the dynamical propagator, should allow for much larger timesteps for the outer loops in multiple timestep methods [105].

An area where the authors feel that more work is needed in terms of characterizing the behavior of polarizable force fields is with respect to the prediction of vapor–liquid equilibria across a range of state points; this effectively speaks to the phase transferability of such force fields. It is widely accepted in the modeling community that point charge based polarizable force fields are not competitive with fixed-charge force fields in terms of prediction of phase-equilibria. The evidence for this comes from parameterizations of polarizable force fields that use molecular polarizabilities that are scaled down from the gas-phase values. Though this scaling arises from a practical need to avoid "polarization catastrophes" in the condensed phase, one can reasonably question whether the application of a reduced polarizability across both phases is accurate. As has been suggested before, polarizable models parameterized with condensed phase properties at ambient conditions cannot recover the loss of attractive electrostatic interactions as the critical point is approached, unlike fixed-charge force fields for which the charge–charge interaction (which captures the total electrostatic interaction) retains the full attractive contribution far into the low density regime. However, the physics of these systems requires that the polarizability of

the gas-phase (or low-density phases) must increase. We suggest revisiting phase-equilibria of small molecule systems with the goal of allowing some variation of the molecular polarizability with phase in order to explore whether polarizable models, with a more accurate representation of the variation of polarizability across phases, can indeed accurately predict phase equilibria. Work addressing this issue continues in our laboratory.

Acknowledgements

The authors acknowledge generous financial support from the National Science Foundation (Grant No. MCB-0413858) and National Institutes of Health (Center for Research Resources at the Pittsburgh Supercomputer Center) (Grant No. RR06009).

References

[1] A.R. Leach. *Molecular Modelling Principles and Applications*, Pearson Education Limited, Essex, England (2001).
[2] T.A. Halgren, W. Damm. Polarizable force fields. *Curr. Opin. Struct. Biol.*, **11**, 236 (2001).
[3] S. Patel, A.D. MacKerell Jr., C.L. Brooks III. CHARMM fluctuating charge force field for proteins: II protein/solvent properties from molecular dynamics simulations using a non-additive electrostatic model. *J. Comp. Chem.*, **25**, 1504 (2004).
[4] S. Patel, C.L. Brooks III. CHARMM. Fluctuating charge force field for proteins: I. Parameterization and application to bulk organic liquid simulations. *J. Comp. Chem.*, **25**, 1 (2004).
[5] P. Ren, J.W. Ponder. Consistent treatment of inter- and intramolecular polarization in molecular mechanics calculations. *J. Comp. Chem.*, **23**, 1497 (2002).
[6] P. Ren, J.W. Ponder. Polarizable atomic multipole water model for molecular mechanics simulation. *J. Phys. Chem. B*, **107**, 5933 (2003).
[7] G. Lamoureux, A.D. MacKerell, B. Roux. A simple polarizable model of water based on classical drude oscillators. *J. Chem. Phys.*, **119**, 5185 (2003).
[8] A. Grossfield, P. Ren, J.W. Ponder. Ion solvation thermodynamics from simulation with a polarizable force field. *J. Am. Chem. Soc.*, **125**, 15671 (2003).
[9] J. Gao, D. Habibollazadeh, L. Shao. A polarizable intermolecular potential function for simulation of liquid alcohols. *J. Phys. Chem.*, **99**, 16460 (1995).
[10] S.W. Rick, S.J. Stuart. Potentials and algorithms for incorporating polarizability in computer simulations. In *Reviews in Computational Chemistry*, K.B. Lipkowitz, D.B. Boyd (Eds.), pp. 89, John Wiley and Sons Inc., New York (2002).
[11] S.W. Rick, B.J. Berne. Dynamical fluctuating charge force fields: the aqueous solvation of amides. *J. Am. Chem. Soc.*, **118**, 672 (1996).
[12] S.W. Rick, S.J. Stuart, B.J. Berne. Dynamical fluctuating charge force fields: application to liquid water. *J. Chem. Phys.*, **101**, 6141 (1994).
[13] S. Patel, C.L. Brooks III. A nonadditive methanol force field: Bulk liquid and liquid–vapor interfacial properties via molecular dynamics simulations using a fluctuating charge model. *J. Chem. Phys.,* 122 (2005).
[14] G.A. Kaminski, H.A. Stern, B.J. Berne, R.A. Friesner. Development of an accurate and robust polarizable molecular mechanics force field from *ab initio* quantum chemistry. *J. Phys. Chem. A*, **108**, 621 (2004).
[15] N. Gresh. Energetics of Zn^{2+} binding to a series of biologically relevant ligands: a molecular mechanics investigation grounded on *ab initio* self-consistent field supermolecule computations. *J. Comp. Chem.*, **16**, 856 (1995).
[16] N. Gresh, D.R. Garmer. Comparative binding energetics of Mg^{2+}, Ca^{2+}, Zn^{2+}, and Cd^{2+} to biologically relevant ligands: combined *ab initio* SCF supermolecule and molecular mechanics investigation. *J. Comp. Chem.*, **17**, 1481 (1996).
[17] M. Ledecq, F. Lebon, F. Durant, C. Giessner-Prettre, A. Marquez, N. Gresh. Modeling of copper(II) complexes with the SIBFA polarizable molecular mechanics procedure. Application to a new class of HIV-1 protease inhibitors. *J. Phys. Chem. B*, **107**, 10640 (2003).
[18] J.W. Ponder. TINKER, Version 4.2. Washington University, School of Medicine. (2004).
[19] B. Thole. *Chem. Phys.*, **59**, 341 (1981).
[20] P.T.v Duijnen, M Swart. *J. Phys. Chem. A*, **102**, 2399 (1998).
[21] A.K. Rappe, W.A. Goddard III. Charge equilibration for molecular dynamics simulations. *J. Phys. Chem.*, **95**, 3358 (1991).
[22] H.A. Stern, F. Rittner, B.J. Berne, R. Friesner. Combined fluctuating charge and polarizable dipole models: application to a five-site water potential function. *J. Chem. Phys.*, **115**, 2237 (2001).
[23] R.A. Bryce, M.A. Vincent, N.O.J. Malcolm, I.H. Hillier, N.A. Burton. Cooperative effects in the structuring of fluoride water clusters: *ab initio* hybrid quantum mechanical/molecular mechanical model incorporating polarizable fluctuating charge solvent. *J. Chem. Phys.*, **109**, 3077 (1998).
[24] G.A. Kaminski, H.A. Stern, B.J. Berne, R.A. Friesner, Y.X. Cao, R.B. Murphy, R. Zhou, T.A. Halgren. Development of a polarizable force field for proteins via *ab initio* quantum chemistry: first generation model and gas phase tests. *J. Comp. Chem.*, **23**, 1515 (2002).
[25] B. Chen, J.J. Potoff, J.I. Siepmann. Adiabatic nuclear and electronic sampling Monte Carlo simulations in the Gibbs ensemble: application to polarizable force fields for water. *J. Phys. Chem.*, **104**, 2378 (2000).
[26] S.W. Rick, S.J. Stuart, J.S. Bader, B.J. Berne. Fluctuating charge force fields for aqueous solutions. *J. Mol. Liq.*, **65/66**, 31 (1995).
[27] M.C.C. Ribeiro, L.C.J. Almeida. Fluctuating charge model for polyatomic ionic systems: A test case with diatomic anions. *J. Chem. Phys.*, **110**, 11445 (1999).
[28] E. Llanta, K. Ando, R. Rey. Fluctuating charge study of polarization effects in chlorinated organic liquids. *J. Phys. Chem. B.*, **105**, 7783 (2001).
[29] H.A. Stern, G.A. Kaminski, J.L. Banks, R. Zhou, B.J. Berne, R.A. Friesner. Fluctuating charge, polarizable dipole, and combined models: parameterization from *ab initio* quantum chemistry. *J. Phys. Chem. B*, **103**, 4730 (1999).
[30] S.W. Rick, B.J. Berne. Free energy of the hydrophobic interaction from molecular dynamics simulations: the effects of solute and solvent polarizability. *J. Phys. Chem. B*, **101**, 10488 (1997).
[31] N. Yoshii, R. Miyauchi, S. Miura, S. Okazaki. A molecular-dynamics study of the equation of state of water using a fluctuating-charge model. *Chem. Phys. Lett.*, **317**, 414 (2000).
[32] B. Chen, J.I. Siepman. Monte Carlo algorithms for simulating systems with adiabatic separation of electronic and nuclear degrees of freedom. *Theor. Chem. Acc.* (1999).
[33] S.W. Rick. Simulations of ice and liquid water over a range of temperatures using the fluctuating charge model. *J. Chem. Phys.*, **114**, 2276 (2001).
[34] R. Chelli & Procacci, P. A transferable polarizable electrostatic force field for molecular mechanics based on the chemical potential equalization principle. *J Chem Phys.,* **117**, 9175 (2002).
[35] R.G. Parr, W. Yang. *Density-Functional Theory of Atoms and Molecules*, Oxford University Press, Oxford (1989).
[36] R.T. Sanderson. An interpretation of bond lengths and a classification of bonds. *Science*, **114**, 670 (1951).
[37] R.T. Sanderson. *Chemical Bonds and Bond Energy*, Academic Press, New York (1976).
[38] R.F. Nalewajski, J. Korchowiec, Z. Zhou. Molecular hardness and softness parameters and their use in chemistry. *Int. J. Quantum Chem.: Quantum Chem. Symp. 22*, **22**, 349 (1988).
[39] S. Nose. *Mol. Phys.*, **52**, 255 (1984).
[40] H.C. Andersen. *J. Chem. Phys.*, **72**, 2384 (1980).
[41] M. Parrinello, A. Rahman. *Phys. Rev. Lett.*, **45**, 1196 (1980).
[42] R. Car, M. Parrinello. Unified approach for molecular dynamics and density-functional theory. *Phys. Rev. Lett.*, **55**, 2471 (1985).
[43] G. Pastore, E. Smargiassi, F. Buda. Theory of *ab initio* molecular-dynamics calculations. *Phys. Rev. A*, **44**, 6334 (1991).

[44] Y.-P. Liu, K. Kim, B.J. Berne, R.A. Friesner, S.W. Rick. Constructing *ab initio* force fields for molecular dynamics simulations. *J. Chem. Phys.*, **108**, 4739 (1998).
[45] P.R. Rablen, J.W. Lockman, W.L. Jorgensen. *Ab initio* study of hydrogen-bonded complexes of small organic molecules with water. *J. Phys. Chem. A*, **102**, 3782 (1998).
[46] C.M. Breneman, K.B. Wiberg. Determining atom-centered monopoles from molecular electrostatic potentials, the need for high sampling density in formamide conformational analysis. *J. Comp. Chem.*, **11**, 361 (1990).
[47] L.E. Chirlian, M.M. Francl. Charges fit to electrostatic potentials. *J. Comp. Chem.*, **8**, 894 (1987).
[48] M.J. Frisch, G.W. Trucks, H.B. Schlegel, G.E. Scuseria, M.A. Robb, J.R. Cheeseman, J.A. Montgomery Jr., T. Vreven, K.N. Kudin, J.C. Burant, J.M. Millam, S.S. Iyengar, J. Tomasi, V. Barone, B. Mennucci, M. Cossi, G. Scalmani, N. Rega, G.A. Petersson, H. Nakatsuji, M. Hada, M. Ehara, K. Toyota, R. Fukuda, J. Hasegawa, M. Ishida, T. Nakajima, Y. Honda, O. Kitao, H. Nakai, M. Klene, X. Li, J.E. Knox, H.P. Hratchian, J.B. Cross, V. Bakken, C. Adamo, J. Jaramillo, R. Gomperts, R.E. Stratmann, O. Yazyev, A.J. Austin, R. Cammi, C. Pomelli, J. Ochterski, P.Y. Ayala, K. Morokuma, G.A. Voth, P. Salvador, J.J. Dannenberg, V.G. Zakrzewski, S. Dapprich, A.D. Daniels, M.C. Strain, O. Farkas, D.K. Malick, A.D. Rabuck, K. Raghavachari, J.B. Foresman, J.V. Ortiz, Q. Cui, A.G. Baboul, S. Clifford, J. Cioslowski, B.B. Stefanov, G. Liu, A. Liashenko, P. Piskorz, I. Komaromi, R.L. Martin, D.J. Fox, T. Keith, M.A. Al-Laham, C.Y. Peng, A. Nanayakkara, M. Challacombe, P.M.W. Gill, B. Johnson, W. Chen, M.W. Wong, C. Gonzalez, J.A.G. Pople. Gaussian, Inc., Wallingford, CT. (2004)
[49] A.D. MacKerell Jr., D. Bashford, M. Bellott, R.L. Dunbrack Jr, J.D. Evanseck, M.J. Field, S. Fischer, J. Gao, H. Guo, S. Ha, D. Joseph-McCarthy, L. Kuchnir, K. Kuczera, F.T.K. Lau, C. Mattos, S. Michnick, T. Ngo, D.T. Nguyen, B. Prodhom, W.E. Reiher III, B. Roux, M. Smith, J.C. Smith, R. Stote, J. Straub, M. Watanabe, J. Wiorkiewicz-Kuczera, D. Yin, M. Karplus. All-atom empirical potential for molecular modeling and dynamics studies of proteins. *J. Phys. Chem. B*, **102**, 3586 (1998).
[50] D. Yin, A.D. MacKerell Jr. Combined ab intio/empirical approach for optimization of Lennard–Jones parameters. *J. Comp. Chem.*, **19**, 334 (1998).
[51] W.L. Jorgensen, D.S. Maxwell, J. Tirado-Rives. Development and testing of the OPLS all-atom force field on conformational energetics and properties of organic liquids. *J. Am. Chem. Soc.*, **118**, 11225 (1996).
[52] W.L. Jorgensen, J. Tirado-Rives, The O.P.L.S. Force field for proteins: energy minimizations for crystals of cyclic peptides and crambin. *J. Am. Chem. Soc.* 1657 (1988).
[53] W.L. Jorgensen, J.M. Briggs, L. Contreras. Relative partition coefficients for organic solutes from fluid simulations. *J. Phys. Chem.* 1683 (1990).
[54] M.P. Allen, D.J. Tildesley. *Computer Simulation of Liquids*, Clarendon Press, Oxford (1987).
[55] G.J. Martyna, M.L. Klein, M. Tuckerman. *J. Chem. Phys.*, **97**, 2635 (1992).
[56] T. Darden, D. York, L. Pederson. Particle mesh Ewald: An $N\log(N)$ method for Ewald sums in large systems. *J. Chem. Phys.*, **98**, 10089 (1993).
[57] T. Darden, U. Essman, H. Lee, L. Perera, M.L. Berkowitz, L. Pederson. A smooth particle mesh Ewald method. *J. Chem. Phys.*, **103**, 8577 (1995).
[58] S.W. Rick. In *Simulation and Theory of Electrostatic Interactions in Solution: Computational Chemistry, Biophysics, and Aqueous Solutions*, L.R. Pratt, G. Hummer (Eds.), American Institute of Physics, Santa Fe, New Mexico (1999).
[59] T.M. Nymand, P. Linse. Molecular dynamics simulations of polarizable water at different boundary conditions. *J. Chem. Phys.*, **112**, 6386 (2000).
[60] P. Roychowdhury, B.S. Basak. The crystal structure of indole. *Acta Cryst. B*, **31**, 1559 (1975).
[61] I.J. Bruno, J.C. Cole, P.R. Edgington, M. Kessler, C.F. Macrae, P. McCabe, J. Pearson, R. Taylor. New software for searching the Cambridge structural database and visualizing crystal structures. *Acta Cryst. B*, **58**, 389 (2002).
[62] M.E. Tuckerman, M. Parrinello. Integrating the Car–Parrinello equations. I. Basic integration techniques. *J. Chem. Phys.*, **101**, 1302 (1994).
[63] J.A. Izaguirre, S. Reich, R.D. Skeel. Longer time steps for molecular dynamics. *J. Chem. Phys.*, **110**, 9853 (1999).
[64] M.E. Tuckerman, B.J. Berne. Molecular dynamics algorithm for multiple time scales: systems with disparate masses. *J. Chem. Phys.*, **94**, 1465 (1990).
[65] P.E. Blochl, M. Parrinello. Adiabaticity in first-principles molecular dynamics. *Phys. Rev. B*, **45**, 9413 (1992).
[66] P.E. Blochl. Second generation wave-function thermostat for *ab-initio* molecular dynamics. *Phys. Rev. B*, **65**, 104303 (2001).
[67] L.R. Olano, S.W. Rick. Fluctuating charge normal modes: an algorithm for implementing molecular dynamics simulations with polarizable potentials. *J. Comp. Chem.*, **26**, 699 (2005).
[68] H. Liu, M. Elstner, E. Kaxiras, T. Frauenheim, J. Hermans, W. Yang. Quantum Mechanics Simulation of Protein Dynamics on Long Timescale. *Proteins: Struct Funct Genet*, **44**, 484 (2001).
[69] S. Saka, D. Kusdiana. Biodiesel fuel from rapeseed oil as prepared in supercritical methanol. *Fuel*, **80**, 225 (2001).
[70] M. Genta, F. Yano, Y. Kondo, W. Matsubara and S. Oomoto. Mitsubishi Heavy Industries, Ltd. 2003.
[71] M. Matsumoto, Y. Kataoka. Molecular orientation near liquid–vapor interface of methanol: simulational study. *J. Chem. Phys.*, **90**, 2398 (1988).
[72] P.B. Miranda, Y.R. Shen. Liquid interfaces: a study by sum-frequency vibrational spectroscopy. *J. Phys. Chem. B*, **103**, 3292 (1999).
[73] K.R. Wilson, R.D. Schaller, D.T. Co, R.J. Saykally, B.S. Rude, T. Catalano, J.D. Bozek. Surface relaxation in liquid water and methanol studied by X-ray absorption spectroscopy. *J. Chem. Phys.*, **117**, 7738 (2002).
[74] C.J. Benmore, Y.L. Loh. The structure of liquid ethanol: a neutron diffraction and molecular dynamics study. *J. Chem. Phys.*, **112**, 5877 (2000).
[75] T. Yamaguchi, C.J. Benmore, A.K. Soper. The structure of subcritical and supercritical methanol by neutron diffraction, empirical potential structure refinement, and spherical harmonic analysis. *J. Chem. Phys.*, **112**, 8976 (2000).
[76] S. Dixit, J. Crain, W.C.K. Poon, J.L. Finney, A.K. Soper. Molecular segregation observed in a concentrated alcohol-water solution. *Nature*, **416**, 829 (2002).
[77] S.Y. Noskov, G. Lamoureux, B. Roux. Molecular dynamics study of hydration in ethanol–water mixtures using a polarizable force field. *J. Phys. Chem.* (2005).
[78] C. Wick, L.X. Dang. Investigating pressure effects on structural and dynamical properties of liquid methanol with many-body interactions. *J. Chem. Phys.*, **123**, 184503 (2005).
[79] A. Morita. Water polarizability in condensed phase *ab initio* evaluation by cluster approach. *J. Comp. Chem.*, **23**, 1466 (2002).
[80] P. Jungwirth, D.J. Tobias. Ions at the air/water interface. *J. Phys. Chem. B*, **106**, 6361 (2002).
[81] P. Paricaud, M. Predota, A.A. Chialvo, P.T. Cummings. From dimer to condensed phases at extreme conditions: accurate predictions of the properties of water by a Gaussian charge polarizable model. *J. Chem. Phys.*, **122**, 244511 (2005).
[82] T.W. Allen, O.S. Andersen, B. Roux. Energetics of ion conduction through the gramicidin channel. *PNAS*, **101**, 117 (2004).
[83] S. Edwards, B. Corry, S. Kuyucak, S-H. Chung. Continuum electrostatics fails to describe ion permeation in the gramicidin channel. *Biophys. J.*, **83**, 1348 (2002).
[84] B. Roux, M. Karplus. Potential energy function for cation–peptide interactions: an *ab initio* study. *J. Comp. Chem.*, **16**, 690 (1995).
[85] S. Berneche, B. Roux. Molecular dynamics of the KcsA K+ channel in a bilayer membrane. *Biophys. J.*, **78**, 2900 (2000).
[86] I.H. Shrivastava, D.P. Tieleman, P.C. Biggin, M.S.P. Sansom. K+ versus Na+ ions in a K channel selectivity filter: a simulation study. *Biophys. J.*, **83**, 633 (2002).
[87] I.H. Shrivastava, M.S.P. Sansom. Simulations of Ion Permeation through a Potassium Channel Molecular Dynamics of KcsA in a Phospholipid Bilayer (2000).
[88] L.E. Townsley, W.A. Tucker, S. Sham, J.F. Hinton. Structures of gramicidin A, B, and C incorporated into sodium dodecyl sulfate micelles. *Biochemistry*, **40**, 11676 (2001).
[89] F. Tian, K-C. Lee, W. Hu, T.A. Cross. Monovalent cation transport: lack of structural deformation upon cation binding. *Biochemistry*, **35**, 11959 (1996).

[90] D.W. Urrey. The gramicidin A transmembrane channel: a proposed π_{LD} helix. *Proc. Natl. Acad. Sci.*, **68**, 672 (1971).
[91] K.A. Duca, P.C. Jordan. Comparison of selectively polarizable force fields for ion–water–peptide interactions: ion translocation in a gramicidin-like channel. *J. Phys. Chem.*, **102**, 9127 (1998).
[92] A.D. MacKerell Jr., B. Brooks, C.L. Brooks III, L. Nilsson, B. Roux, Y. Won, M. Karplus. CHARMM: the energy function and its parametrization with an overview of the program. In *Encyclopedia of Computational Chemistry*, P.V.R. Schleyer, N.L. Allinger, T. Clark, J. Gasteiger, P.A. Kollman, H.F. Schaefer III, P.R. Schreiner (Eds.), Vol. 1, pp. 271, John Wiley & Sons, Chichester (1998).
[93] B.R. Brooks, R.E. Bruccoleri, B.D. Olafson, D.J. States, S. Swaminathan, M. Karplus. CHARMM: a program for macromolecular energy, minimization, and dynamics calculations. *J. Comp. Chem.*, **4**, 187 (1983).
[94] S.J. Marrink, F. Jahnig, H.J. Berendsen. Proton transport across transient single-file water pores in a lipid membrane studied by molecular dynamics simulations. *Biophys. J.*, **71**, 632 (1996).
[95] V.M. Anisimov, G. Lamoureux, I.V. Vorobyov, N. Huang, B. Roux, D. Alexander, J. MacKerell. Determination of electrostatic parameters for a polarizable Force field based on the classical drude oscillator. *J. Chem. Theory Comput.*, **1**, 153 (2005).
[96] S. Patel, C.L. Brooks III. Revisiting the hexane–water interface via molecular dynamics simulations using non-additive alkane–water potentials, *manuscript submitted* (2005).
[97] J.-P. Douliez, A. Leonard, E.J. Duforc. Restatement of order parameters in biomembranes: calculation of C–C bond order parameters from C–D quadrupolar splitting. *Biophys. J.*, **68**, 1727 (1995).
[98] T.B. Woolf, B. Roux. Structure, energetics, and dynamics of lipid–protein interactions: a molecular dynamics study of the gramicidin A channel in a DMPC bilayer. *Proteins: Struct. Funct Genet.*, **24**, 92 (1996).
[99] A. van der Vaart, B.D. Bursulaya, C.L. Brooks III, K.M. Merz Jr. Are many-body effects important in protein folding? *J. Phys. Chem. B*, **104**, 9554 (2000).
[100] A. van der Vaart, V. Gogonea, S.L. Dixon, K.M. Merz Jr. Linear scaling molecular orbital calculations of biological systems using the semiempirical divide and conquer method. *J. Comp. Chem.*, **21**, 1494 (2000).
[101] I.V. Vorobyov, V.M. Anisimov, D. Alexander, J. MacKerell. Polarizable empirical force field for alkanes based on the classical drude oscillator model. *J. Phys. Chem. B* (2005).
[102] J.L. Banks, G.A. Kaminski, R. Zhou, D.T. Mainz, B.J. Berne, R.A. Friesner. Parametrizing a polarizable force field from *ab initio*. I. The fluctuationg point charge model. *J. Phys. Chem.*, **110**, 741 (1999).
[103] W.L. Jorgensen, J. Tirado-Rives. Potential energy functions for atomic-level simulations of water and organic and biomolecular systems. *PNAS*, **102**, 6665 (2005).
[104] M. Shirts, J.W. Pitera, W.C. Swope, V.S. Pande. Extremely precise free energy calculations of amino acid side chain analogs: Comparison of common molecular mechanics force fields for proteins. *J. Chem. Phys.*, **199**, 5740 (2003).
[105] R. Zhou, E. Harder, H. Xu, B.J. Berne. Efficient multiple time step method for use with Ewald and particle mesh Ewald for large biomolecular systems. *J. Chem. Phys.*, **115**, 2348 (2001).
[106] W.L. Jorgensen. Optimized intermolecular potential functions for liquid alcohols. *J. Phys. Chem.*, **90**, 1276 (1986).
[107] J.W. Caldwell, P.A. Kollman. Structure and properties of neat liquids using nonadditive molecular dynamics: water methanol, and *N*-methylacetamide. *J. Phys. Chem.*, **99**, 6208 (1995).
[108] L.X. Dang, T-M. Chang. Many-body interactions in liquid methanol and its liquid/vapor interface: a molecular dynamics study. *J. Chem. Phys.*, **119**, 9851 (2003).
[109] R.C. Wilhoit, B.J. Zwolinski. *J. Phys. Chem. Ref. Data.*, (Suppl. 2) (1973).
[110] E.V. Ivash, D.M. Dennison. *J. Chem. Phys.*, **21**, 1804 (1953).
[111] C.L. Yaws. *Thermodynamic and Physical Property Data*, Gulf Publishing Company, Houston (1992).
[112] A.L. McClellan. *Tables of Experimental Dipole Moment*, Rahara Enterprises, El Cerrito (1989).